

Higher order mass aggregation terms in a nonlinear predator-prey model maintain limit cycle stability in Saturn's F ring

Omar El Deeb *

July 26, 2024

Abstract

We consider a generic higher order mass aggregation term for interactions between particles exhibiting oscillatory clumping and disaggregation behavior in the F ring of Saturn, using a novel predator-prey model that relates the mean mass aggregate (prey) and the square of the relative dispersion velocity (predator) of the interacting particles. The resulting cyclic dynamic behavior is demonstrated through time series plots, phase portraits and their stroboscopic phase maps.

Employing an eigenvalue stability analysis of the Jacobian of the system, we find out that there are two distinct regimes depending on the exponent and the amplitude of the higher order interactions of the nonlinear mass term. In particular, the system exhibits a limit cycle oscillatory stable behavior for a range of values of these parameters and a non-cyclic behavior for another range, separated by a curve across which phase transitions would occur between the two regimes. This shows that the observed clumping dynamics in Saturn's F ring, corresponding to a limit cycle stability regime, can be systematically maintained in presence of physical higher order mass aggregation terms in the introduced model.

1 Introduction

Saturn, the sixth planet from the Sun in our solar system, is known for its distinct appearance and its prominent ring system that spans a diameter of approximately 280,000 kilometers and sets it apart from other planets. With its pale yellow hue, Saturn boasts a massive atmosphere primarily composed of hydrogen and helium. Composed mainly of ice particles and rocky debris, the rings consist of countless individual ringlets, each with its own characteristics and unique patterns. They consist of countless particles, ranging in size from tiny grains to large chunks of ice and rock. The origin of Saturn's rings remains a topic of scientific debate, but they are believed to be the result of various processes, including the breakup of moons or the remnants of a shattered moon that got too close to the planet and was torn apart by tidal forces [1, 2]. The rings are categorized into several main divisions, such as the bright and broad A, B, and C rings, with the Cassini Division separating the A and B rings. Additionally, fainter and narrower rings, such as the F and G rings, exist within the system. They lie in the Roche zone where the accretion is limited by Saturn's tidal force and particle collisions [3].

The F ring was initially discovered by the Pioneer 11 spacecraft in 1979 [4]. It is a narrow and faint ring located at about 3000 km outside the main ring system of Saturn, with a semi-major axis of about 140,000 km. Analyses of the observed back-scattered signal from the Hubble Space telescope, Voyager observations and other ground based observations reveal that this ring is mainly composed of dust that constitutes about 80 – 98% of its particle fraction [5], in addition to icy particles. These observations also reveal that it exhibits a complex and ever-changing structure. It is exceptionally thin, with an average width of about 30 kilometers and consists of multiple strands and braids of material that weave in and out, creating intricate patterns and knots [6, 7]. These structures are constantly evolving due to the gravitational interactions

*Department of Mathematics, University of Warwick, Coventry, United Kingdom

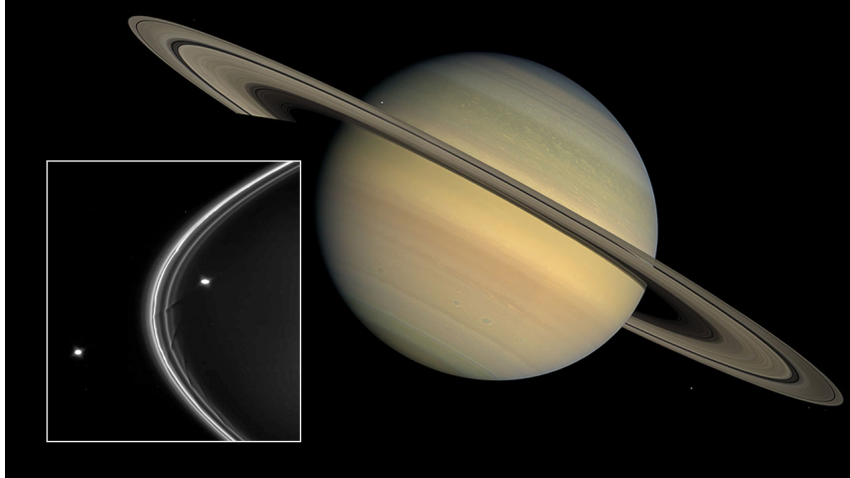


Figure 1: An image of Saturn and its rings. The zoomed image shows the F ring with its nearest moons: Prometheus (inside ring) and Pandora (outside ring). Image credits: NASA/JPL/Space Science Institute.

between the ring particles and Saturn’s moons [8], particularly the moon Prometheus, which orbits just inside the ring.

The Cassini spacecraft had a primary objective of studying Saturn, its rings and its moons in great detail. Launched in 1997, Cassini arrived at Saturn in 2004 and embarked on an extensive investigation of the planet and its surroundings. It studied Saturn’s ring system, exploring its structure, origin, and various divisions [9, 10] and also conducted a thorough examination of Saturn’s diverse moons, such as Titan and Enceladus, investigating their geological features, compositions, and interactions with Saturn’s magnetosphere. Its images revealed multiple strands, braids, and clumps of material within the F ring, showcasing its complex patterns. Related studies showed that the particles had size distributions on several magnitudes across the ring, ranging from micrometers up to the order of kilometer in size [11, 12]. The spacecraft also captured the gravitational interactions between the F ring and Saturn’s shepherd moons, mainly the larger and nearer Prometheus and then Pandora, which influenced its shape and confinement. The two moons are shown in the zoomed image in Fig. (1) in the neighborhood of the F ring [13]. Cassini detected temporary radial structures called spokes composed of levitated dust particles and observed denser regions known as knots within the F ring. Furthermore, the mission unveiled the interactions between the F ring and nearby moons, highlighting their impact on the ring’s dynamics, leading to disturbances, streamers, and localized concentrations of material [14, 15]. Cassini’s observations of heavily disturbed areas during occultations reveal compelling indications of clustering [16]. The observed clustering can be understood as a process of aggregation followed by disaggregation, occurring over time spans ranging from hours to weeks. The disruption of these clusters might be a result of high-velocity collisions that cause fragmentation or the shedding of loose fragments due to tidal forces. Additionally, the presence of moons could contribute to the aggregation process by causing congestion along their path, leading to increased collisions [17].

Recent studies reported strong evidence of presence of moonlets within the ring’s bright core. They showed that ongoing gravitational and collisional effects of small satellites combined with the perturbative effects of Prometheus, the largest and closest moon in the neighborhood of the F ring, are responsible for the resulting structure of the F ring and its continual collisions and dynamics occurring on an almost daily basis [18]. The mean aggregate mass fluctuations were explained through a system of coupled differential relating mass aggregation and fragmentation with changes in relative dispersion velocities of these particles through a predator-prey model [19].

These types of models, also known as Lotka-Volterra models [20, 21], are mathematical models used to study the interactions between predator and prey populations. The models consist of a set of differential equations that describe the population dynamics of predators and prey over time. They assume that the

predator population’s growth depends on the availability of prey, while the prey population’s growth is influenced by predation. In a basic predator-prey model, there are two variables: the population sizes of the predator species and the prey species. Initially, an increase in prey population leads to more resource availability for predators, causing the predator population to grow. As the predator population increases, it exerts more predation pressure on the prey, causing the prey population to decline. With fewer prey available, the predator population eventually decreases. As a result, the reduced predation allows the prey population to recover, starting the cycle again. Predator-prey models were initially introduced in the study of ecological systems, however, they are currently employed in various models in fields that exhibit similar behavior, ranging from particle dynamics to conservation biology, financial markets and economics [22, 23, 24, 25, 26, 27, 28, 29].

However, predator-prey models introduced in the literature to study the particle interaction dynamics in the rings of Saturn do not accommodate for the possibility of higher order mass aggregation terms through non-linear mass exponents in the model. Nonlinear prey terms in the predator-prey model are important because they capture the realistic dynamics of predator-prey interactions natural systems, where the relationship between predators and prey dynamics is not simply linear. Nonlinear prey terms can introduce various dynamics such as predator saturation, oscillations, and stable coexistence of predator and prey populations. By incorporating nonlinear prey terms, the predator-prey model can better reflect the complexities of natural systems and provide insights into the population dynamics and interactions in a more realistic manner [30]. Recent studies have shown that the addition of nonlinear loss terms to the Lotka-Volterra model in dust-forming plasmas stabilizes the oscillatory behavior in the populations of particles in the plasma and better explains the observed experimental behavior [31].

Our paper aims to broaden the scope of the previous predator-prey model based simulations of Saturn’s F ring and fill the current gap in the literature by introducing a higher order interaction term for mass aggregation with a generic nonlinear exponent, and study the conditions under which the solutions would still exhibit limit cycle oscillations around an equilibrium that can resemble the dynamics corresponding to actual observations of clumping, spokes and knots across Saturn’s F ring.

The paper is organized as follows: after the introduction section, we construct our modified Lotka-Volterra model for the mean aggregate mass dynamics in the F rings of Saturn in section 2. We explain the methods required to analytically solve the system for some particular cases, and the procedure to numerically solve the system for a generic choice of parameters. In section 3, we present our results and discuss them. We finally conclude in section 4.

2 The Model

The pioneering work in [19] introduced a predator-prey model for clumping triggered by moons in the rings of Saturn. The ring response periods vary on a time scale comparable to the synodic period of the forcing of Prometheus. This model describes the long term behavior of the ring dynamics based on gains and losses of the particle masses and their relative velocities due to coagulation and fragmentation interplay.

The coagulation term representing mass growth in [19] was approximated to grow in time in the form of $\frac{dM}{dt} = \frac{M}{T}$. In this approximation, $T = \frac{T_{orb}}{4\tau}$ is the collision period, T_{orb} is the orbital period and τ is the optical depth at a specific location. In this paper, we consider an additional modified generic growth term which includes a non-linear mass dependence kM^n , with a nonlinear mass amplitude k and a degree n to account for a more general and accurate approximation and a possible higher order growth pattern in particle coagulation. The physical processes leading to such nonlinearity could be attributed to numerous forms of interaction. Gravitational compression and inelastic collisions enhance local density and stabilize clumps, while gravitational instabilities cause small density perturbations to exponentially grow due to self-gravity. Shear reversal traps particles in areas of reduced relative velocity because of differential rotation, and swing amplification increases the amplitude of spiral density waves as they interact with the disk’s rotation. Together, these mechanisms could introduce nonlinear terms resulting in the complex behavior seen in Saturn’s rings.

Parameter	Value	Comments
T_{orb}	1	All times are scaled with respect to T_{orb}
τ	0.1	Optical depth
T	$\frac{T_{orb}}{4\tau}$	Estimated period of collisions
ϵ	0.6	Normal coefficient of restitution
M_0	$2 \times 10^9 \text{g}$	Calculated for a 10m aggregate with density $\rho = 0.5 \text{ g/cm}^3$
v_{esc}	0.5 m/s	The escape velocity on the surface of M_0
T_{syn}	$112 T_{orb}$	The forcing period of Prometheus on the F ring
A_0	$\in [0.1, 1]$	Amplitude of the moon driving force
v_{th}	$v_{th}^2 = \frac{A_0 T_{syn}}{2\pi}$	Threshold velocity for sticking

Table 1: Parameters used for the numerical solutions of the modified predator-prey model with non linear mass terms in the F ring.

Mass fragmentation occurs due to collisions of particles that reach a relative velocity greater than the aggregates sticking threshold. The mass loss due to fragmentation was found to be proportional to the square of the relative velocity dispersion v_{rel} and the particle masses, such that $\frac{dM}{dt} = -\frac{V}{v_{th}^2} \frac{M}{T}$, where $V = v_{rel}^2$ and v_{th} is a parameter representing the threshold velocity for sticking.

The temporal evolution of the relative velocity dispersion has a term related to the losses caused by collisional dissipation. It is expressed by $\frac{dV}{dt} = -\frac{V(1-\epsilon^2)}{T}$, where ϵ is the normal coefficient of restitution. On the other hand, local and non-local viscous stirrings contribute a velocity growth term of the form $\frac{dV}{dt} = \frac{M^2}{M_0^2} \frac{v_{esc}^2}{T_{orb}}$ where v_{esc} is the escape velocity from the surface of a reference mass M_0 . In addition, moon perturbations in the F ring, caused by Prometheus, contribute an external forcing term with synodic angular frequency $\omega = \frac{2\pi}{T_{syn}}$, and synodic period T_{syn} .

Consequently, taking into account all of these contributions, we obtain a predator-prey model with a set of coupled nonlinear differential equations that describe the time development of each of $M(t)$ and $V(t)$.

$$\begin{cases} \frac{dM}{dt} = \frac{M}{T} - \frac{V}{v_{th}^2} \frac{M}{T} + kM^n \\ \frac{dV}{dt} = -\frac{(1-\epsilon^2)}{T} V + \frac{M^2}{M_0^2} \frac{v_{esc}^2}{T_{orb}} - A_0 \cos(\omega t) \end{cases} \quad (1)$$

The time in these equations is scaled with respect to the orbital period, hence $T_{orb} \equiv 1$. A_0 is the amplitude of the moon forcing term, with $A_0 = \frac{2\pi v_{th}^2}{T_{syn}}$. A summary of all parameters and their numerical values is presented in Table 1.

The system of coupled differential equations represents a predator-prey model describing the mass fluctuations in the F ring of Saturn with moon perturbations, with a generic non-linear higher order mass term. In this context, the mean aggregate mass represents the prey population whereas the square of the velocity dispersion represents the predator population. The predator (relative velocity dispersion) grows larger as the mass aggregates grow. But as it grows, more collisions would occur on higher velocity scales causing increased fragmentation of the aggregates, hence limiting its prey. This has similar qualitative dynamics as ecological predator-prey systems, but with a unique quantitative nature due to the simultaneous presence of a predator driving force, a predator squared mass term and a generic prey non-linear mass term.

The equilibrium points of this system correspond to the solution of

$$\frac{dM}{dt} = \frac{dV}{dt} = 0 \quad (2)$$

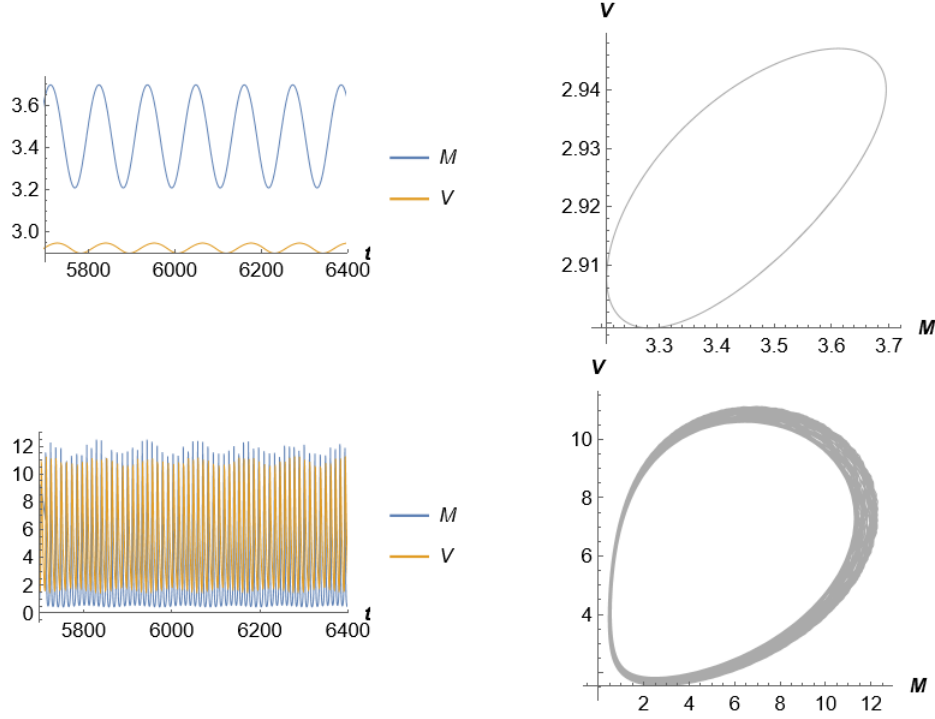


Figure 2: Time series plots and phase plots of M and V , showing distinct dynamic behavior for $k = 0.15, n = 1.2$ (up) & $k = 0.6, n = 1.3$ (bottom). Parameters: $T_{syn} = 112$ periods, $v_{esc} = 0.5$ m/s, $M_0 = 2 \times 10^9 g$, $A_0 = \tau = 0.1$, $\epsilon = 0.6$ and initial conditions $M(0) = 4.5 \times 10^9 g$ and $V(0) = 3m^2/s^2$.

In the limiting case of a negligible driving force $A_0 \rightarrow 0$, the equilibrium points, reached after amplitude death occurrence, could be obtained from the solution of:

$$\begin{cases} \frac{M}{T} \left(1 - \frac{V}{v_{th}^2} + kTM^{n-1} \right) = 0 \\ -\frac{(1-\epsilon^2)}{T}V + \frac{v_{esc}^2}{M_0^2}M^2 = 0 \end{cases} \quad (3)$$

We can show that, upon reaching equilibrium, the square of the relative velocity would be proportional to the mean aggregate mass:

$$V = \frac{Tv_{esc}^2}{(1-\epsilon^2)M_0^2}M^2 \quad (4)$$

leading to the relation:

$$1 - \frac{Tv_{esc}^2}{(1-\epsilon^2)v_{th}^2M_0^2}M^2 + kTM^{n-1} = 0 \quad (5)$$

This is a polynomial of order $n - 1$. It can be exactly solved for some particular cases as in $n = 1, 2$ or 3 . The corresponding solutions are given by:

$$\begin{cases} M^* = \frac{(1+kT)(1-\epsilon^2)v_{th}^2M_0^2}{Tv_{esc}^2} = \frac{v_{th}M_0}{v_{esc}} \sqrt{\left(k + \frac{1}{T}\right)(1-\epsilon^2)} & n = 1 \\ M^* = \frac{(1-\epsilon^2)M_0^2 \left(kT + \left(k^2T^2 + \frac{4Tv_{esc}^2}{(1-\epsilon^2)M_0^2v_{th}^2} \right) v_{th}^2 \right)}{2Tv_{esc}^2} & n = 2 \\ M^* = \left(\frac{Tv_{esc}^2}{(1-\epsilon^2)v_{th}^2M_0^2} - kT \right)^{-1/2} & n = 3 \end{cases} \quad (6)$$

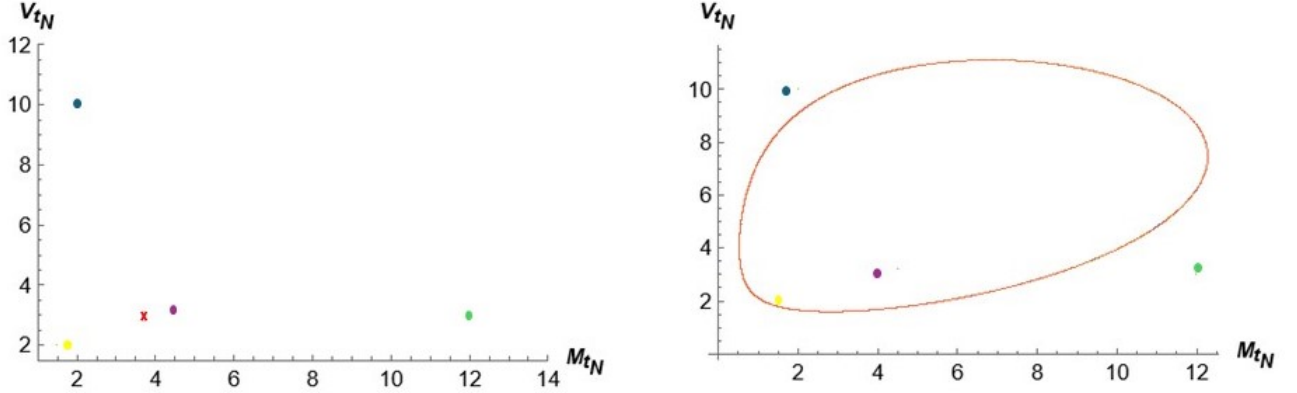


Figure 3: Stroboscopic phase space plots of $(M(t_N), V(t_N))$ at $t = NT_{syn}$ for $k = 0.15, n = 1.2$ (left) & $k = 0.6, n = 1.3$ (right) for 4 different initial conditions denoted by circular dots. On the left, all orbits reduce to a single point (red x), while on the right, all orbits fall into a closed cycle path.

Whereas the velocities could be simply obtained by substituting these solution back in Eq. (4). However, analytical solutions are not attainable in presence of the moon driving force, and for a generic n case.

To numerically solve this system, we adopt the following method. Stability analysis requires linearising the modified predator-prey system with $A_0 = 0$ in (3) around the equilibrium points. We determine the Jacobian of the system represented by the matrix:

$$J = \begin{pmatrix} \frac{1}{T} \left(1 - \frac{V^*}{v_{th}^2} \right) + nk (M^*)^{n-1} & -\frac{M^*}{v_{th}^2 T} \\ \frac{2v_{esc}^2}{M_0^2} M^* & -\frac{1-\epsilon^2}{T} \end{pmatrix} \quad (7)$$

We determine the eigenvalues λ of the Jacobian, which allow us to determine the behavior and the stability of the system. For a generic values of n and k , we start by numerically solving Eq. (5), to determine the corresponding values of M . We require that $M > 0$ for physical solutions. Then, for each (n, k) , we substitute n, k and M in (7) to compute λ .

3 Results and discussions

We numerically solve the coupled system of non-linear differential equations presented in Eq. (1) for various sets of parameters. We plot the obtained solutions of the mean mass aggregate M and the square of the relative dispersion velocity V as a function of time, simultaneously in Fig. (2) for the following parameters: $T_{syn} = 112$ orbital periods, $v_{esc} = 0.5$ m/s, $M_0 = 2 \times 10^9 g$, $A_0 = 0.1$, $\epsilon = 0.6$, $\tau = 0.1$ and initial conditions $M(0) = 4.5 \times 10^9 g$ and $V(0) = 3 m^2/s^2$. This is done in two distinct dynamic regimes, for $k = 0.15, n = 1.2$ (top) and for $k = 0.6, n = 1.3$ (bottom). We also plot their corresponding phase space plot showing a continuous parametric plot of $V(t)$ with respect to $M(t)$.

We observe that for a certain range of combinations of the nonlinear coupling k and power n , a periodic oscillation emerges with a period identical to that of the perturbing synodic period. This is shown in Fig.2 (top). On the other hand, a more complicated dynamic behavior emerges for another range of values of k and n . A sample plot is shown in Fig.2 (bottom). We can notice the presence of two patterns of frequencies, with rapid and slow oscillations. The plots also show that the two variables under consideration are not in phase. The mean mass aggregate $M(t)$ (prey) peaks before the square of the dispersion velocity $V(t)$ (predator), as expected for a predator lagging a prey's population.

To understand the true nature of this dynamic behavior, we have to analyze the system by studying its stroboscopic map, with periodic snapshots of $M(t)$ and $V(t)$ taken at a $t_N = \frac{2\pi N}{\omega} = NT_{syn}$, for integer N . The corresponding phase space maps are plotted for 4 initial conditions $(M(0), V(0)) =$

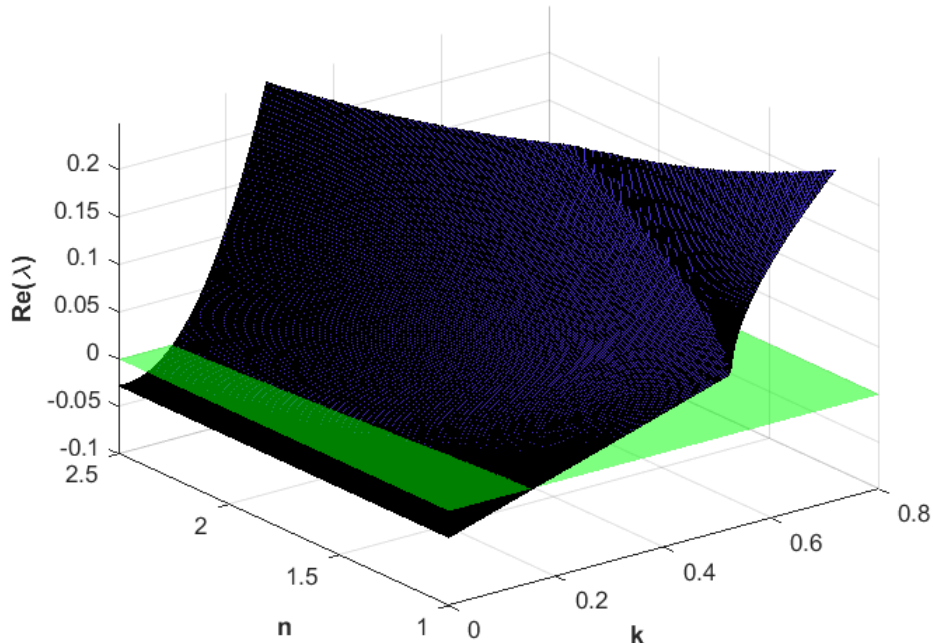


Figure 4: The real part of an eigenvalue of the Jacobian in Eq.7 ($A_0 = 0$), for parameters set to same values as in Fig. 2, plotted in navy blue. The green plane corresponds to the (n, k) plane or $Re(\lambda) = 0$.

$(1.5, 2)$, $(2, 10)$, $(4.5, 3.2)$ and $(12, 2)$, for $k = 0.15, n = 1.2$ (left) and $k = 0.6, n = 1.3$ (right). The figures show that for the former pair of nonlinear coupling and exponent, the orbit immediately reduces to a single point in the phase space after the first iteration, denoted by the red x in the figure. While for the latter parameters, using identical initial conditions, the corresponding stroboscopic phase plots reduce to a closed elliptical orbit, as shown in Fig. 3 (right).

With these stroboscopic maps, we can differentiate two types of periodic orbit in the full system. The case of $k = 0.15, n = 1.2$ shown in Fig. 3 (top) represents a periodic orbit which is Floquet-stable. It asymptotically tends toward the stable fixed point, representing a central periodic orbit with no limit cycle in this case. Whereas for the case of $k = 0.6, n = 1.3$, we witness the emergence of a closed orbit limit cycle in the stroboscopic map. This represents the appearance of a limit torus in the full flow. The phase transition from a fixed point to a periodic orbit in the stroboscopic map indicates the occurrence of a quasi periodic Hopf bifurcation at a particular critical value of the pair (k, n) .

To further explore the critical values of (k, n) that lead to Hopf bifurcation, we consider the unperturbed system (Eq. 3) with $A_0 = 0$ and analyze its eigenvalues. Different (k, n) parameterizations of the amplitude and exponent parameters of the non-linear coagulation could lead to attracting stable fixed points or to limit cycle behaviour. We classify the stability regions with respect to (k, n) values by employing a stability analysis of the Jacobian of the system.

After numerically solving Eq. (7), we present a three dimensional plot of $Re(\lambda)$, the real part of the eigenvalue λ of the Jacobian, with respect to n and k in Fig. (4). We obtain two distinct regions for $Re(\lambda) \neq 0$. The (n, k) plane corresponds to $Re(\lambda) = 0$. It is plotted in green color in Fig. 4. Solutions below the (n, k) plane are due to attracting fixed points while those above the plane are due to limit cycle solutions. Transitions across the line of intersection of $Re(\lambda)$ and the (n, k) plane correspond to quasi periodic Hopf bifurcations, hence the birth of limit cycles, combined with the condition $Im(\lambda) \neq 0$.

To specify the solutions leading to $Im(\lambda) = 0$, we choose a large set of (k, n) such that $0 \leq k \leq 2.2$ and $1 \leq n \leq 2.6$ with an iteration of an increment of 0.025 between consecutive values of each parameter. We

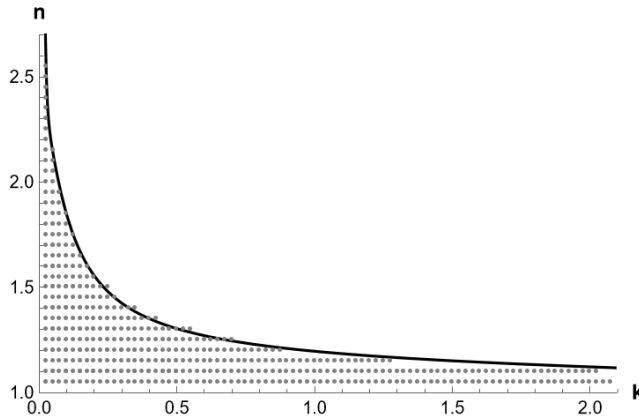


Figure 5: A scatter plot of (k, n) values (gray dots) corresponding to $Im(\lambda) < 0$ for $A_0 = 0$. The black line is a regression fit of the values at the edges of the scatter plot corresponding to $Im(\lambda) = 0$. The region above the line (white region) corresponds to $Im(\lambda) > 0$

solve the modified Lotka-Volterra system presented in Eq. (1) iteratively for all of these values, plot their corresponding curves like those in Fig. (2), and graphically deduce which ones correspond to $Im(\lambda) < 0$. The (k, n) leading to this type of solutions are marked with gray dots in the scatter plot in Fig. (5). The black line in that figure is a plot of a polynomial regression fit of the edge values of the scatter plot. It represents a boundary line emerging from $Im(\lambda) = 0$.

Physically, our results imply that the actual cyclic stability in Saturn’s F rings can be maintained for a range of couplings k and exponents n of a higher order mass aggregation term.

A sample image taken by Cassini [35] in Fig. (6) reveals bright clumps of aggregated material on the edge of the F ring in addition to fine structures and streams within its core. The process of disaggregation due to rapid collisions prohibits further growth of particles, and keeps the system in cyclic equilibrium. This is in line with previous studies [36] that analyzed particle size distribution within the F ring and found out that they are characterized by an inverse power law of the form:

$$n(s) = n(s_0) \left(\frac{s}{s_0} \right)^{-q} \quad (8)$$

where s is the particle size, s_0 is a reference particle size, and n is the number of particles.

Our results show that a nonlinear mass aggregation term can preserve all the dynamical features corresponding to actual clumping, aggregations and disaggregations that prohibit further mass growth in the ring and that the associated cyclic stability could be maintained for a well defined region of values of the exponent and the amplitude of the nonlinear mass growth term.

4 Conclusions

The F ring is one of the most dynamic rings of Saturn, with variable changes occurring on relatively short timescales. Prometheus has a central role in triggering formations of streams, collisions and clumps.

In this study, a generic higher order mass aggregation term was considered for particle interactions in the F ring of Saturn leading to aggregation, disaggregation and clumping. A modified predator-prey model was used to simulate the interactions of the prey and the predator variables, namely: the mean mass aggregate and the relative dispersion velocities of the particles.

An eigenvalue stability analysis of the Jacobian of the system revealed the existence of two distinct regimes depending on the exponent and amplitude of the higher order interactions of the nonlinear mass term. We explored the limit cycle oscillatory stable behavior for a range of values of these parameters separated by a curve across which phase transitions could occur into a distinct region of amplitude death or instability. This work showed that the observed dynamical changes in Saturn’s F rings and their limit

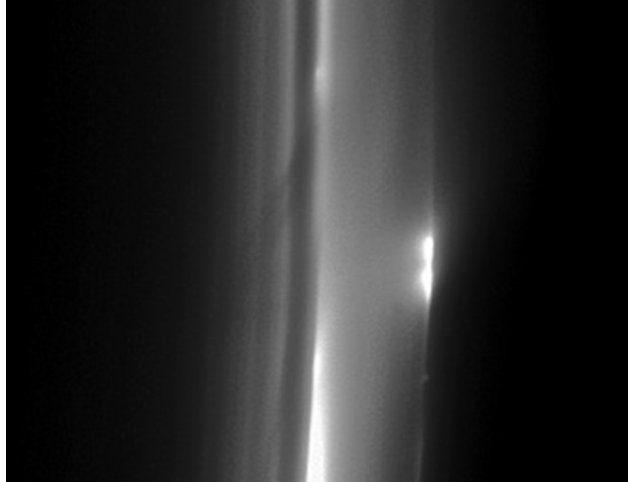


Figure 6: Actual bright clumps, fine structures and streams in Saturn's F rings. Image Credit: NASA/JPL/SSI

cycle stability features could be systematically maintained in the presence of higher order mass aggregation terms in the novel predator-prey model.

Acknowledgments

The author acknowledges the valuable and insightful comments by two anonymous reviewers.

References

- [1] R.M. Canup, Origin of Saturn's rings and inner moons by mass removal from a lost Titan-sized satellite, *Nature* 468, 943-946 (2010). doi: 10.1038/nature09661.
- [2] K. Lumme, On the formation of Saturn's rings, *Astrophysics and Space Science* 15, 404-414 (1972). doi: 10.1007/BF00649769.
- [3] M. Tiscareno, M. Hedman, J. Burns & J. Castillo-Rogez, Compositions and Origins of Outer Planet Systems: Insights from the Roche Critical Density, *The Astrophysical Journal Letters* 765:2 (2013). doi: 10.1088/2041-8205/765/2/L28.
- [4] T. Gehrels, L.R. Baker, E. Beshore, et al., Imaging Photopolarimeter on Pioneer Saturn, *Science* 207 (4429), 434-439 (1980). doi: 10.1126/science.207.4429.434.
- [5] F. Poulet, B. Sicardy, C. Dumas, et al., The crossings of Saturn ring plane by the earth in 1995: ring thickness, *Icarus* 145, 147-165 (2000). doi: doi.org/10.1006/icar.1999.6314.
- [6] R. Hanel, B. Conrath, et al., Infrared Observations of the Saturnian System from Voyager 1. *Science* 212, 4491, 192-200 (1981). doi: 10.1126/science.212.4491.1
- [7] B. Smith, L. Soderblom, et al., Encounter with Saturn: Voyager 1 Imaging Science Results, *Science*, 212, 4491, 163-191 (1981). doi: 10.1126/science.212.4491.163.
- [8] P. Goldreich, S. Tremaine, The Dynamics of Planetary Rings, *Annual Review of Astronomy and Astrophysics* 20, 249-293 (1982). doi: 10.1146/annurev.aa.20.090182.001341.

- [9] A. Nagy, A. Kliore, E. Marouf, et al., First results from the ionospheric radio occultations of Saturn by the Cassini spacecraft, *Journal of Geophysical Research: Space Physics* 111, A6 (2006). doi: 10.1029/2005JA011519.
- [10] D. Harland, *Cassini at Saturn*, Springer Praxis Books, Praxis New York (2007). doi: 10.1007/978-0-387-73978-6.
- [11] M. Hedman, P. Nicholson, M. Showalter, et al., The Christiansen Effect in Saturn’s narrow dusty rings and the spectral identification of clumps in the F ring, *Icarus* 215:2, 695-711 (2011). doi: 10.1016/j.icarus.2011.02.025.
- [12] S. Vahidina, J. Cuzzi, M. Hedman, et al., Saturn’s F ring grains: Aggregates made of crystalline water ice, *Icarus* 215:2, 682-694 (2011). doi: 10.1016/j.icarus.2011.04.011.
- [13] Science, Satellite smashup created Saturn’s narrow F ring (2015), Accessed on: June 12, 2023. Available at: <https://www.science.org/content/article/satellite-smashup-created-saturns-narrow-f-ring>.
- [14] L. Esposito, B. Meinke, J. Colwell, et al., Moonlets and clumps in Saturn’s F ring, *Icarus* 194:1, 278-289 (2008). doi: 10.1016/j.icarus.2007.10.001.
- [15] N. Albers, M. Sremcevic, J. Colwell & L. Esposito, Saturn’s F ring as seen by Cassini UVIS: Kinematics and statistics, *Icarus* 217:1, 367-388 (2012). doi: 10.1016/j.icarus.2011.11.016.
- [16] B. Meinke, L. Esposito, N. Albers & M. Sremcevic, Classification of F ring features observed in Cassini UVIS occultations 218:1, 545-554 (2012). doi: 10.1016/j.icarus.2011.12.020.
- [17] N. Brilliantov, P.L. Krapivsky, A. Bodrova & J. Schmidt, Size distribution of particles in Saturn’s rings from aggregation and fragmentation, *Proceedings of the National Academy of Science* 112:31, 9536-9541 (2015). doi: 10.1073/pnas.1503957112.
- [18] C. Murray, K. Beurle, N. Cooper, et al., The determination of the structure of Saturn’s F ring by nearby moonlets. *Nature* 453, 739–744 (2008). doi: 10.1038/nature06999.
- [19] L. Esposito, N. Albers, B. Meinke, et al., A predator–prey model for moon-triggered clumping in Saturn’s rings, *Icarus* 217:1, 103-114. doi: 10.1016/j.icarus.2011.09.029.
- [20] A. Lotka, Analytical Note on Certain Rhythmic Relations in Organic Systems, *Proceedings of the National Academy of Science* 6:7, 410-415 (1920). doi: 10.1073/pnas.6.7.4.10.
- [21] V. Volterra, Variations and fluctuations of the number of individuals in animal species living together, *Animal Ecology*, McGraw-Hill 412-433 (1931).
- [22] P. Wangersky, Lotka-Volterra Population Models, *Annual Review of Ecology and Systematics* 9, 189-218 (1978). doi:10.1146/annurev.es.09.110178.001201.
- [23] L. Frachebourg, P.L. Krapivsky & E. Ben-Naim, Spatial organization in cyclic Lotka-Volterra systems, *Physical Review E* 54:6, 6186 (1996). doi:10.1103/PhysRevE.54.6186.
- [24] G. Dibeh & O. El Deeb, Synchronization in a market model with time delays, arXiv:2405.00046 (2024). doi:10.48550/arXiv.2405.00046.
- [25] A. Chakrabarti, Stochastic Lotka–Volterra equations: A model of lagged diffusion of technology in an interconnected world, *Physica A: Statistical Mechanics and Its Applications* 442, 214-223 (2016). doi:10.1016/j.physa.2015.09.030.
- [26] Y. Marinkas, R. White & S. Walsh, Lotka–Volterra signals in ASEAN currency exchange rates, *Physica A: Statistical Mechanics and Its Applications* 545, 123743 (2020). doi:10.1016/j.physa.2019.123743.
- [27] G. Dibeh, Contagion effects in a chartist–fundamentalist model with time delays, *Physica A: Statistical Mechanics and Its Applications* 382:1, 52-57 (2007). doi:10.1016/j.physa.2007.02.007.

- [28] T. Ray, L. Moseley & N. Jan, A Predator–Prey Model with Genetics: Transition to a Self-Organized Critical State, *International Journal of Modern Physics C* 9:5, 701-710 (1998), doi: 10.1142/S0129183198000601.
- [29] W. Just, E. Reibold, H. Benner et al., Limits of time-delayed feedback control, *Physics Letters A* 254:3-4, 158-164 (1999). doi: 10.1016/S0375-9601(99)00113-9.
- [30] K. Owolabi, Computational dynamics of predator-prey model with the power-law kernel, *Results in Physics* 21, 103810 (2021). doi: 10.1016/j.rinp.2020.103810.
- [31] A.E. Ross & D.R. McKenzie, Predator-prey dynamics stabilized by nonlinearity explain oscillations in dust-forming plasmas, *Scientific Reports* 6, 24040 (2016). doi: 10.1038/srep24040.
- [32] Q. Shu & J. Xie, Stability and bifurcation analysis of discrete predator–prey model with nonlinear prey harvesting and prey refuge, *Mathematical Methods in the Applied Sciences* 45:7 (2021), 3589-3604. doi:10.1002/mma.8005.
- [33] Y. Tao, Global existence of classical solutions to a predator–prey model with nonlinear prey-taxis, *Nonlinear Analysis: Real World Applications* 11 (2010), 2056-2064. doi:10.1016/j.nonrwa.2009.05.005.
- [34] X. Liu, T. Zhang, X. Meng et al., Turing–Hopf bifurcations in a predator–prey model with herd behavior, quadratic mortality and prey-taxis, *Physica A: Statistical Mechanics and its Applications* 496, 446-460 (2018). doi: 10.1016/j.physa.2018.01.006.
- [35] J. Major, Saturn’s fluctuating F ring, *Phys.org*, (2012). Available at: <https://phys.org/news/2012-11-saturn-fluctuating.html>. Accessed on: June 23, 2023.
- [36] C. Murray & R. French, The F Ring of Saturn. In: M. Tiscareno & C. Murray, *Planetary Ring Systems: Properties, Structure, and Evolution*, Cambridge: Cambridge Univ. Press, 338-362 (2018). doi: 10.1017/9781316286791.013.